



HAL
open science

Combination of ScaRaB-2 and CERES with Meteosat-5 to remove time sampling bias and improve radiation budget estimations in the INDOEX region

M. Viollier, R. Kandel, P. Raberanto

► **To cite this version:**

M. Viollier, R. Kandel, P. Raberanto. Combination of ScaRaB-2 and CERES with Meteosat-5 to remove time sampling bias and improve radiation budget estimations in the INDOEX region. *Journal of Geophysical Research: Atmospheres*, 2004, 109, 10.1029/2003JD003947 . hal-04109997

HAL Id: hal-04109997

<https://hal.science/hal-04109997>

Submitted on 31 May 2023

HAL is a multi-disciplinary open access archive for the deposit and dissemination of scientific research documents, whether they are published or not. The documents may come from teaching and research institutions in France or abroad, or from public or private research centers.

L'archive ouverte pluridisciplinaire **HAL**, est destinée au dépôt et à la diffusion de documents scientifiques de niveau recherche, publiés ou non, émanant des établissements d'enseignement et de recherche français ou étrangers, des laboratoires publics ou privés.

Copyright

Combination of ScaRaB-2 and CERES with Meteosat-5 to remove time sampling bias and improve radiation budget estimations in the INDOEX region

M. Viollier, R. Kandel, and P. Raberanto

Laboratoire de Météorologie Dynamique, Institut Pierre-Simon Laplace, CNRS, Ecole Polytechnique, Palaiseau, France

Received 3 July 2003; revised 10 November 2003; accepted 23 January 2004; published 9 March 2004.

[1] Using data available over the INDOEX area, Meteosat-5 visible and infrared data have been combined with ScaRaB/Resurs and CERES/TRMM broadband data for March 1999, and with CERES/TRMM and CERES/Terra data for March 2000. The study proceeds by collocation of the data sets, comparison of narrowband Meteosat radiances to broadband ScaRaB radiances, and conversion of radiances to fluxes. In the longwave (LW) domain, a multiple regression is found between ScaRaB and CERES fluxes, the two Meteosat infrared channels (infrared window and water vapor) and the viewing zenith angle. In the shortwave (SW) domain, narrowband-to-broadband (NB-BB) and ERBE-like radiance-to-flux conversions are applied. The RMS differences between the ScaRaB/CERES and Meteosat instantaneous flux retrievals are about 10 Wm^{-2} and 40 Wm^{-2} respectively in the LW and SW domains. A large part of these differences comes from the residual coregistration and narrow-band-to-broadband conversion errors. On the contrary, the mean difference or bias between all data sets is very small, consistent at the 1% (LW) and 4% (SW) level. The LW and SW conversion equations have been used to convert Meteosat observations at each half hour into instantaneous broadband flux estimates consistent with the instantaneous CERES flux estimates for the same day. New monthly means are computed in this way: the changes are small in the LW but significant in the SW domain (regional means: $\sim 20 \text{ Wm}^{-2}$, 20°S – 20°N means: $\sim 4 \text{ Wm}^{-2}$), especially for studies of long-term changes. *INDEX TERMS:* 1694 Global Change: Instruments and techniques; 3394 Meteorology and Atmospheric Dynamics: Instruments and techniques; 3360 Meteorology and Atmospheric Dynamics: Remote sensing; 3309 Meteorology and Atmospheric Dynamics: Climatology (1620); *KEYWORDS:* Earth radiation budget, climate, Meteosat

Citation: Viollier, M., R. Kandel, and P. Raberanto (2004), Combination of ScaRaB-2 and CERES with Meteosat-5 to remove time sampling bias and improve radiation budget estimations in the INDOEX region, *J. Geophys. Res.*, *109*, D05105, doi:10.1029/2003JD003947.

1. Introduction

[2] The components of Earth Radiation Budget (ERB) at the “top of the atmosphere” (TOA) are fundamental parameters of the climate system, and since the beginning of the space age, different models of broadband scanning radiometers (BBSR) have been flown on satellites in low Earth orbit in order to measure them. An important objective of such missions is the detection of significant ERB fluctuations on interdecadal or longer timescales [Wielicki *et al.*, 2002]. Following earlier missions described by House *et al.* [1986], the narrow-field-of-view instruments flown over the past twenty years are the scanners of the NASA Earth Radiation Budget Experiment (ERBE) [Barkstrom *et al.*, 1989], the French-Russian-German Scanner for Radiation Budget mission (ScaRaB) [Kandel *et al.*, 1998; Duvel *et al.*, 2001], and the NASA Clouds and the Earth’s Radiant Energy System (CERES) mission [Wielicki *et al.*, 1996].

Such instruments measure radiances reflected and emitted by the Earth-atmosphere system with very high absolute accuracy (of order 1% or better), with satisfactory spatial resolution (10–50 km), but with poor temporal sampling (twice every 24 hours, for a single polar satellite and only once during daytime). Considering the strength of the diurnal cycle, there is a possibility that some of the variation in the long-term record arises from the inevitable changes in sampling times as one Sun-synchronous satellite begins or ceases operation or is replaced by another. By comparison, geostationary satellites (GEO) such as Meteosat observe Earth with excellent spatial resolution and temporal sampling (typically 2.5 km, 30 min), but they lack appropriate onboard calibration sources. Their radiometric gains must be adjusted with vicarious methods, which can provide interinstrument stability (relative accuracy) of 3 to 5% in the visible and 0.3 to 1% in the infrared, as in the satellite intercalibrations of ISCCP [Brest *et al.*, 1997] but poor absolute accuracy, no better than 5 to 10% in the visible and 2% in the infrared. The high radiometric accuracy of ERB

scanners in low Earth orbit (BBSR-LEO) and the excellent space-time sampling of GEO instruments are then strongly complementary. Their intercomparison should serve to improve the GEO radiance calibration and reciprocally the GEO observations may fill the gaps between the coarse BBSR-LEO time series [Young *et al.*, 1998; Haeffelin *et al.*, 1999]. Such GEO interpolations are now being tested and implemented in the CERES data processing.

[3] Whether derived from BBSR-LEO or GEO data, estimation of TOA ERB components must go by way of radiance-to-flux conversions made problematical by the anisotropy of the radiance field. Indeed, the hemispheric flux should be obtained from the integration of outgoing radiances in all directions. However, except for a few instruments (e.g., POLDER; Buriez *et al.* [1997], Loeb *et al.* [2000] and MISR; Diner *et al.* [1999]), narrow-field-of-view instruments on satellites measure instantaneous outgoing radiances in only one direction for each Earth location. Fluxes then are estimated from the BBSR-LEO radiances using empirical or theoretical models of the anisotropy of the radiation field. The ERBE-type algorithms of ScaRaB [Viollier *et al.*, 1995] and CERES [Wielicki *et al.*, 1996] use an empirical angular model based on a 12-scene-type-classification [Suttles *et al.*, 1988; Wielicki and Green, 1989]. This method yields fairly reliable regional and monthly mean values, but it cannot be expected to provide instantaneous flux estimates with high accuracy. It is expected that large individual errors, specifically in the SW, are canceled by the space and time averaging processes, assuming statistical independence of the error sources. For the instantaneous flux estimates, misclassification of scenes can result in erroneous angular corrections [e.g., Ye and Coakley, 1996]. By checking the scene identification with concurrent AVHRR scene analysis, Diekmann and Smith [1989] found that the standard deviation of SW errors due to scene misclassification might be as large as 13%. The auxiliary narrow-band channels of ScaRaB can help the scene identification [Stubenrauch *et al.*, 1993, 2002]. However, even if scene classification is correct, angular corrections use models (in particular bidirectional reflectance distribution functions or BRDF in the SW) which are valid only statistically, and even for a given scene type, there is in fact strong variance in the relation between radiance and flux. This was shown by comparing simultaneous coincident instantaneous regional flux estimates from ERBE scanners on ERBS and NOAA-9 and -10. Dlhopsky *et al.* [1994] found standard deviations of SW differences of 13% for clear and partly cloudy scenes and 9% for mostly cloudy and overcast scenes. In a similar way, Thomas *et al.* [1995] found 10 Wm^{-2} (or 3.5%) in the LW. To reduce such errors, one approach is to increase the number of scene types and the reliability of the scene identification algorithm, assuming that the flux-radiance relationships for such more precisely defined scene types can indeed be shown to exhibit less variance. Indeed, the best recent improvement came from the complementary use of high-resolution imagers on board the same platforms as the CERES broadband scanners, specifically VIRS on TRMM, and MODIS on Terra and Aqua. The narrow-band measurements and relatively high spatial resolutions of these instruments make possible better scene identification inside the CERES FOV, and are the key to the new CERES angular

distribution models [Loeb *et al.*, 2003]. In the absence of high-spatial-resolution narrow-band data from the same LEO platform, combining the BBSR-LEO data with fairly high-resolution data from GEO images in several narrow spectral bands (NBI-GEO) can improve the BBSR scene identification and then the instantaneous flux estimates, although this may be hindered by coregistration errors of data coming from different platforms.

[4] The BBSR-LEO/NBI-GEO comparisons have up to now been carried out using different pairs of instruments, for example: the ERBE and Meteosat scanners [Cheruy *et al.*, 1991b; Vesperini and Fouquart, 1994], ERBE and GOES [Minnis *et al.*, 1991], ScaRaB and Meteosat [Dewitte *et al.*, 1999], ScaRaB and GOES [Trishchenko and Li, 1998], CERES, VIRS, ATSR-2, GOES-8 and GMS-5 [Minnis *et al.*, 2002a, 2002b]. From all these regression analyses, the standard errors of the flux estimates are typically 10 and 40 Wm^{-2} respectively in the LW and SW, and arise from the mismatch errors and from the NB-BB and radiance-to-flux conversions. The largest errors are observed in the SW. This is due to the spatial and temporal variability of the SW radiation field and also because the anisotropy of the SW radiation field is very strong. More recently, Minnis *et al.* [2002a] compared CERES, VIRS, ATSR-2, GOES-8 and GMS-5 radiances and concluded that VIRS (calibrated with an onboard solar diffuser system) can serve as a reliable reference to calibrate the NB imagers on the GEO satellites (NBI-GEO).

[5] In this paper, we analyze data from four additional BBSR-LEO instruments (ScaRaB-2, CERES PFM, FM1 and FM2). In particular, we re-examine the different issues of the BBSR-LEO/NBI-GEO flux combination: the impact of mismatch errors, the radiometric calibration, the narrow-band-to-broadband and the radiance-to-flux conversions which both depend on the scene identification. The data and the problems associated with the coregistration and sampling are discussed in section 2. Sections 3 and 4 respectively present the LW and the SW comparisons of instantaneous radiances and fluxes. The methods for computing monthly means and the comparison with ERBE-type CERES results are given in section 5. The results are summarized in section 6.

2. Data and Methods

2.1. Satellite Data

2.1.1. CERES/TRMM and CERES/Terra

[6] The proto-flight model (PFM) of CERES flew on board the Tropical Rainfall Measurement Mission (TRMM). Both the inclination (35°) and the altitude (350 km) of the TRMM satellite orbit were chosen to optimize the use of the rain radar for tropical studies, yielding an observation cycle of 46 days during which the full diurnal cycle is sampled. The nadir footprint of CERES/TRMM is about 10 km. Data were regularly provided from January to August 1998. After this date, because of technical problems, CERES/TRMM was turned on only for specific experiments, mainly during daytime in March 1999, and for the full month of March 2000. Following this experience with CERES-PFM on TRMM, four CERES flight models (FM) were launched, FM1 and FM2 on board Terra (Sun-synchronous, equator crossing time 10:30) in December 1999, and FM3 and FM4

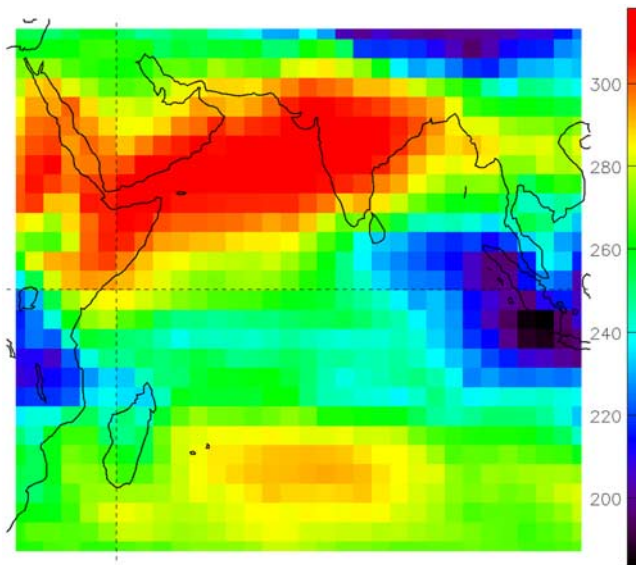


Figure 1. March 2000 monthly means of the LW regional fluxes (CERES/Terra data) over the study area 30°E , 110°E , 35°S , 35°N . The lowest fluxes are found over clouds in the area of the African great lakes, Indonesia, and north of India. Clear sky areas (Arabian Sea and India) give the highest fluxes (Wm^{-2}).

on *Aqua* (Sun-synchronous, equator crossing time 01:30) in May 2002. Thus, between April 2000 and May 2002, only CERES/Terra data were available, and correction for time-sampling bias is essential. On these two Sun-synchronous satellites (705 km altitude), the nadir footprint of the CERES instruments is about 20 km. The TOA flux estimates are available, both using ERBE-like algorithms (ES8 product) and using the new CERES angular model (Single Scan Footprint or SSF product, *Loeb et al.* [2003]). Alternatively, one instrument is used for cross-track scanning, along-track, or in rotating azimuth plane mode. We have used CERES/TRMM data for March 1999 (Transient-Ops2 ERBE-like product, ES8) and 2000 (Edition 2), and the FM1 and FM2 (Edition 1) Terra/ES8 products for March 2000. The Transient-Ops version refers to the CERES/TRMM period during which instrument operations were substantially reduced to conserve instrument life. In spite of interruptions and ensuing thermal nonequilibrium, the effective gain of the instruments did not change by more than 0.5%. When, in the framework of INDOEX, the European geostationary satellite *Meteosat-5* was shifted in 1998 to a position over the Indian Ocean, it became possible to monitor diurnal variations of reflected SW and emitted LW radiation in the tropical Indian Ocean area. This study uses *Meteosat-5* data limited to the area: 30°E , 110°E , 35°S , 35°N ; see the maps of the SW and LW monthly means on Figures 1 and 2. Thus we focus on an area whose geographical and climatological characteristics differ, even in the nonmonsoon month of March, from the areas of GOES/ERBE and *Meteosat*/ERBE studies, the Americas and Africa respectively.

2.1.2. ScaRaB-2

[7] Flying on board the Russian *Resurs* satellite [*Duvel et al.*, 2001], the ScaRaB-2 instrument was a cross-track scanning radiometer with a swath of about 1800 km. The *Resurs* orbit was Sun-synchronous with equator crossing

time (ascending node) 22:30. The ScaRaB onboard calibration system uses multiple sources (blackbody simulators and three sets of lamps). Calibration also has been checked using geophysical cross-calibration between the total and SW channels [*Duvel and Raberanto*, 2000]. The estimated calibration uncertainty is of order 2% or better (1% in the LW). Coincident and collocated CERES and ScaRaB observations have also been found consistent to within 0.5% and 1.5% in the LW and SW domains respectively [*Haeffelin et al.*, 2001]. Together with other instrument characteristics, the ScaRaB spectral bands are given in Table 1.

2.1.3. Meteosat-5

[8] In support of the INDOEX campaigns, *Meteosat-5* was moved in spring 1998 from its initial position (over the Greenwich meridian off Africa) to the Indian Ocean (63°E). As with other meteorological satellite imagers, the (first-generation) *Meteosat* scanning narrow-band radiometer (SR) was first of all designed to provide images of cloud patterns. Accurate absolute calibration was not a priority. Infrared calibration is provided, but the reference blackbody cannot be monitored through the complete optical system. For the visible, there is no onboard calibration system, so only numerical counts are available. The *Meteosat-5* SR has 3 channels: visible (0.3–1.1 μm), infrared window (IR) (10.5–12.5 μm) and infrared water vapor (WV) (5.7–7.5 μm). We have used the “full resolution” *Meteosat* data set (2.5 and 5 km in VIS and IR/WV respectively) specifically prepared by LMD (J. L. Monge, Climserv database, <http://climserv.lmd.polytechnique.fr/>) for INDOEX.

2.2. Collocation Error Impact

[9] Due to cloud inhomogeneities and rapid changes, spatial and temporal variability of the radiation field is very

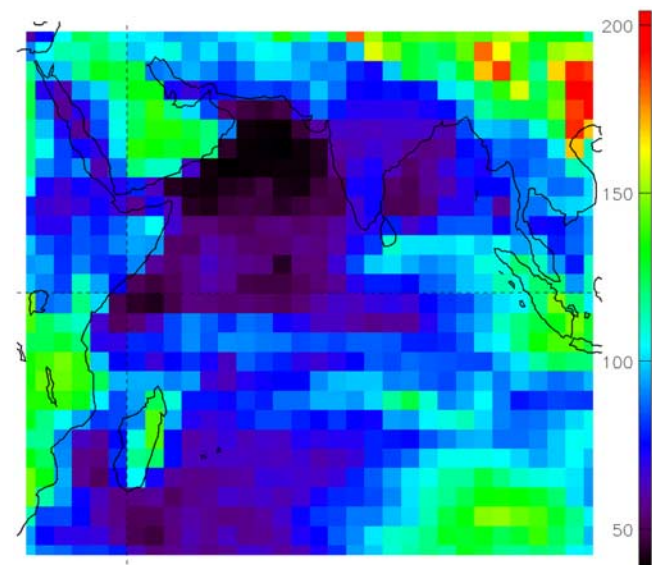


Figure 2. Same as Figure 1 but for the reflected SW flux. The lowest fluxes are found over clear-sky ocean (Arabian Sea, southern ocean off Madagascar, etc.). High fluxes (in green) are observed over cloudy areas (Indonesia, African great lakes, etc.) and desert (Arabia). In red, very high reflected fluxes are observed over southern China (Kwangsi), corresponding to low warm clouds not visible on the LW map (Figure 1).

Table 1. Main Characteristics of the Five Instruments Used in This Paper

Instrument/Satellite	Broadband, μm	Visible, μm	Infrared, μm	Nadir Footprint, km	Orbit
ScaRaB/Resurs	0.2–4 0.2–50	0.55–0.65	10.5–12.5	45	Sun-synchronous 10:30
CERES/TRMM PFM	0.2–4 0.2–50	no	8–12	10	precessing
CERES/Terra FM1 and FM2	0.2–4 0.2–50	no	8–12	20	Sun-synchronous 10:30
Meteosat-5 SR	no	0.3–1.1 (maximum at 0.65)	10.5–12.5 (IR) 5.7–7.1 (WV)	2.5 (Vis) 5 (IR)	geosynchronous

strong, hindering comparisons between instruments on different platforms. We first present simulations of the effects of coregistration errors and of differences in pixel-viewed areas on radiance comparisons. Although we have averaged Meteosat data over the footprint sizes of CERES on TRMM and on Terra and that of ScaRaB/Resurs, these assemblages of Meteosat pixels cannot be identical to the CERES or ScaRaB footprints. To assess the impact of this, we have compared the averages with averages computed with data shifted by 2.5, 5, and 10 km. We also compare two consecutive Meteosat time slots to simulate an error of 30 min in the time coregistration. The results (Table 2) show that the error impact increases rapidly with mismatch, and in the case of SW data from Terra, the radiance error reaches $20 \text{ Wm}^{-2}\text{sr}^{-1}$ (21%) for a location error of 15 km, and about the same for a 30-min error. The LW errors are of the same order, but much lower in relative terms (7%, where in this paper, the relative errors are always defined as the ratio of the RMS error to the average of the radiances or fluxes considered in the data set). Nominal absolute location accuracy is 5 km for CERES and 20 km for ScaRaB, and generally better than 10 km for Meteosat [Desormeaux *et al.*, 1993]. However, assuming a mean location uncertainty of 15 km between the two instruments, Table 2 shows that the corresponding RMS errors cannot be smaller than 13 and $20 \text{ Wm}^{-2}\text{sr}^{-1}$ for the ScaRaB and CERES/Terra footprints. Such large mismatch errors for an intercomparison data set are inherent in use of data from instruments on different satellites not flying in close formation.

[10] In order to reduce the influence of mismatch, it may be useful to compare radiances and fluxes only over homogeneous areas. These are defined here by standard deviation less than 10% over a certain surface. For example, by selecting an area of four footprints, we reduce the RMS difference of the SW ScaRaB case from 12.7 to 2.3 Wm^{-2} (from 12.9 to 6.2 Wm^{-2} in the LW, see the 15-km columns of Table 2). However, this selection strongly affects the scene sampling. Most of the clear areas (land and ocean)

remain in the data set. On the contrary, occurrences of areas of cloud, thus with the highest SW radiance values, are reduced by a large factor. As already noted by *Vesperini and Fouquart* [1994], the selection of homogeneous areas changes the results of the regressions. However, although it is specifically in areas changing from cloudy to clear or vice versa that one needs GEO information on short-term variations, areas of highly reflecting homogeneous cloud should suffice to define the regressions correctly. Another problem arises from the strong correlation between neighboring pixels. The estimates of RMS errors by means of least squares estimators are not correctly obtained when the data are highly temporally and spatially autocorrelated [Li and Leighton, 1992]. We have tried different data sampling methods such as taking one out of ten columns and lines, or one out of twenty, or sampling the (columns but with a random start on each line). The differences were however smaller than those due to the selection of homogeneous areas. Only fairly small differences are found (2%) between regressions with different sampling conditions, an indication of the accuracy of the intercomparisons.

2.3. Differences in Viewing Geometry

[11] The viewing geometries of CERES and ScaRaB differ radically from that of Meteosat. From a geostationary satellite, a given area of Earth is always observed with the same viewing zenith angle (VZA). On the contrary, due to the orbit shift from one day to the next, the viewing angles from a polar or other LEO satellite constantly change. The radiance depends on this angle, especially in the SW domain, where the reflected radiance often exhibits strong dependence on the relative directions of the observed point and the incidence of the Sun's rays (solar zenith angle SZA and relative Sun-target azimuth RA). Computed from VZA, SZA, and RA, two angles play a major role in the anisotropy of the reflected radiation: the scattering angle γ and the angle α from the line of specular reflection. The most obvious aspect of the SW anisotropy is sunglint over the

Table 2. Simulation of Time and Space Coregistration Errors on the BBSR Radiance Comparisons Using Meteosat-5 Data^a

BBR	Nadir Footprint, km	RMS Radiance Differences, $\text{Wm}^{-2}\text{sr}^{-1}$						
		SW			LW			
		2.5 km	5 km	15 km	30 min	5 km	15 km	30 min
CERES/TRMM	10	6.0	11.3	24.1	22.8	9.2	22.0	23.7
CERES/Terra	20	4.0	7.8	19.6	18.9	6.8	18.2	20.8
ScaRaB/Resurs	45	2.3	4.5	12.7	13.1	4.5	12.9	16.1

^aTo simulate spatial errors, Meteosat-5 SR pixels were shifted by 2.5, 5, and 10 km and then averaged over the BBSR footprint. For temporal error simulation, comparison is done between two consecutive 30-min interval images (with solar zenith angle correction in SW). The corresponding SW and LW radiance means were 86 and $270 \text{ Wm}^{-2}\text{sr}^{-1}$, respectively (2000, March 01, slot 17).

Table 3. Differences Between the CERES and METEOSAT-5 LW Flux Estimates^a

CERES Instrument	Flux Mean, Wm ⁻²	<i>r</i>	Differences CERES- Meteosat-5		Sample Size
			Mean, Wm ⁻² %	RMS, Wm ⁻² %	
TRMM 1999 03 all	268.3	0.955	+2.53 (+0.81)	15.72 (7.48)	2 376 698
TRMM 2000 03–4 days	269.1	0.956	+2.37 (+0.64)	13.37 (6.67)	2 211 561
TERRA FM1 2000 03–4 days	269.7	0.963	+1.66 (+0.46)	18.28 (5.94)	1 189 175
TERRA FM2 2000 03–4 days	268.7	0.960	+0.52 (+0.08)	19.17 (6.07)	1 217 825

^aThe Meteosat-5 fluxes are computed according to equation (1) and coefficients found from ScaRaB/Meteosat comparisons in March 1999. The RMS difference level is mainly due to mismatch errors. The mean differences or biases are small (<1%) whatever the instrument.

ocean, which is observed when α is close to zero. For the Meteosat-5 observations coincident with ScaRaB, sunglint is strongly observed in the eastern part (Bay of Bengal). The western part (Arabian Sea and East African coasts) is seen in the course of successive orbits of ScaRaB, 2 or 3 hours later, with the same VZA (fixed GEO geometry), the same mean SZA (due to the ScaRaB/Resurs Sun-synchronism), but with a different RA which yields a larger α and as a result weaker sunglint. For the ScaRaB data, sunglint is always observed at the middle of the western part of the scan line. Our coincident and collocated points are thus observed from the two instruments with different viewing geometry relative to the Sun incidence. In most cases, the two instruments sample totally different aspects of the anisotropy of the reflected flux. Radiances are comparable only if the observation angles are almost identical, which occurs only in a few cases.

3. Instantaneous Fluxes: LW Domain

[12] Since the Meteosat SR has two thermal infrared channels, attempts have been made to estimate the broadband LW flux directly from these two channels, without passing by a scene identification stage. With objectives and data similar to this study, and using simultaneous collocated Meteosat-2 (located at 0°, 0°) and ERBE data for 23 November 1984, *Cheruy et al.* [1991a] found regressions for estimating the LW flux (F_{LW} in Wm⁻²) from the infrared and water vapor radiances (L_{IR} and L_{WV} in Wm⁻²sr⁻¹) with standard deviation of order 10 Wm⁻² or less. The best results were obtained with the following equation

$$F_{LW} = A_0 + A_1 L_{IR} + A_2 L_{IR}^3 + A_3 L_{IR} / \cos(VZA) + A_4 L_{WV} + A_5 L_{WV}^2, \quad (1)$$

where VZA is the viewing zenith angle and accounts for the limb-darkening effect. With this formula, the standard deviation of the flux retrieval typically drops to 10 Wm⁻² ($R^2 = 0.95$), compared to 15 Wm⁻² ($R^2 = 0.90$) for the simple one-channel regression. The same multiple regression has been applied here to the ScaRaB/Meteosat-5 collocated and near-simultaneous data set (620,800 individual data from January to March 1999), yielding the following coefficients: $A_0 = 65.479$, $A_1 = 14.192$, $A_2 = -0.0079$, $A_3 = 1.8412$, $A_4 = 61.33$, $A_5 = -11.03$. Though not identical, these coefficients are similar to those found by *Cheruy et al.* [1991a] correlating ERBE fluxes with coincident but time-interpolated ISCCP B2 data for April 1985. For the 3-month ScaRaB/Meteosat-5 data set

considered here, the regression coefficient is $R^2 = 0.941$ and the standard deviation 9.45 Wm⁻². Equation (1), with the above coefficients, was used by *Roca et al.* [2002] to characterize the radiation, humidity and cloudiness environment of deep convection over the Indian Ocean.

[13] With rigorously the same equation and coefficients, the Meteosat-5 flux estimates have been compared to CERES PFM in March 1999, and to PFM, FM1, and FM2 in March 2000. The results are shown in Table 3. The biases are less than 3 Wm⁻² or 1%. Note that the TRMM bias is consistent with the negative LW difference of ScaRaB minus CERES (-0.8%) found by *Haefelin et al.* [2001]. Overall, this 1% agreement is remarkable since it shows mutual consistency and stability of six IR radiance measurements from five different instruments.

4. Instantaneous Fluxes: SW Domain

4.1. Spectral Correction

[14] The SW analysis requires two steps. The first is the comparison between the narrow-band and broadband radiances; the second is the flux estimation. The relation between NB and BB radiances is mostly sensitive to surface cover type (ocean, land, desert...) and SZA [*Li and Trishchenko*, 1999; *Duvel et al.*, 2000], and only moderately to atmospheric parameters. The narrow-band-to-broadband conversion has also been studied by *Dewitte* [1997]. Using theoretical simulations, he found that correction factors of 1.0, 0.96, 0.84 and 0.88 have to be applied to the VIS signal of METEOSAT-5 for clear-sky desert, land, ocean, and cloud scenes respectively. The correction factor does not significantly change with SZA between 0 and 45° (range of variation for ScaRaB in this study). These results mean that the SW radiances estimated with Meteosat-5, without spectral correction, are underestimated for land and desert compared to clouds and ocean. Note that *Dewitte* [1997] obtained different results for Meteosat-2, whose spectral response is shifted from the blue by 0.1 μ m compared to Meteosat-5. Using the 530 theoretical spectral signatures of *Viollier et al.* [1995], we have checked these results, and we also observe that Meteosat-5 and the visible channel of ScaRaB have about the same SW spectral correction. Consequently, we seek a linear regression between SW radiance L_{SW} and Meteosat visible channel numerical count N_{vis} , with the following equation

$$L_{SW} = a.S.N_{vis} + b, \quad (2)$$

where S is the spectral correction taking into account the spectral correction factor SCF_{scene} for clear ocean, land and

Table 4. Regression Between the SW and VIS Channels of ScaRaB/Resurs in March 1999, With Geodependent Spectral Corrections^a

	Population Size	Mean, $\text{Wm}^{-2}\text{sr}^{-1}$	$\text{SCF}_{\text{scene}}$	A	B	r	RMS, $\text{Wm}^{-2}\text{sr}^{-1}$
Desert	84 143	93.98	1.1	3.495	9.83	0.986	5.6
Land	122 792	122.79	1.05	3.338	15.91	0.989	5.21
Ocean	422 890	62.30	0.95	3.532	6.90	0.998	3.22
All with geodependent spectral correction	629 825	71.67				0.996	4.50
All with simple regression	629 825	71.67		3.62	8.84	0.991	6.83

^aSee equations (2) and (3).

desert. By normalizing $\text{SCF}_{\text{scene}} = 1$ for clouds, a combination of these four basic scenes is used for mixed cloudy scene, so that the general form of S is

$$S = (1 - f)\text{SCF}_{\text{geo}} + f, \quad (3)$$

where f is the cloud fraction (0.025, 0.275, 0.725 and 0.975 respectively for the four ERBE cloud categories, clear, partly cloudy, mostly cloudy and overcast).

[15] In order to estimate the usefulness of equations (2) and (3), and to determine SCF_{geo} empirically, we start by looking for a regression between radiances and flux estimates from both ScaRaB VIS and SW channels, free from multisatellite coregistration errors. The best linear regression has been sought for each geotype by varying the SCF factor by steps of 0.05 between 0.8 and 1.1. The results are summarized in Table 4. By applying equations (2) and (3) with these coefficients, the RMS difference between radiances is 4.5 Wm^{-2} ($r = 0.996$) compared to 6.83 when using a unique regression, i.e., an improvement of 50%. Without the S correction, the corresponding RMS difference would be $5.05 \text{ Wm}^{-2}\text{sr}^{-1}$ meaning an improvement of only 35% compared to the case without any scene discrimination. The values of $\text{SCF}_{\text{scene}}$ 1.1, 1.05 and 0.95 found for desert, land, and ocean, with 1 (by normalization) for overcast cloud, vary in the same sense as Dewitte's theoretical values, meaning a similar underestimation of land and desert radiances. Because of this consistency and the real improvement found from the ScaRaB analysis, the scene-dependent relations with spectral correction defined by equation (3) are used in the ScaRaB, CERES and Meteosat-5 intercomparisons.

[16] Finally, different comparisons between flux retrievals from the ScaRaB VIS and SW channels are presented in Table 5. The first line shows that the SW fluxes retrieved from the SW radiances without angular correction have an RMS error of 19.5 Wm^{-2} . The following lines show that the absence of NB to BB conversion leads to the same error. When applying both NB-BB conversion and angular correction, the SW fluxes retrieved from the VIS radiances have an RMS error of 15 Wm^{-2} (last line), a factor two improvement compared to line 2 (no correction at all).

4.2. Comparisons Between ScaRaB-CERES and Meteosat-5 Flux Estimations

[17] A linear fit is first sought between the ScaRaB flux and the Meteosat-5 numerical count. According to equation (2) and because b is close to zero, the linear fit should have the following form

$$F_{\text{sw}} = A \cdot ((\pi S \cdot N_{\text{vis}})/R) + B, \quad (4)$$

where F_{sw} is the ScaRaB flux, N_{vis} is the Meteosat numerical count averaged over the BBSR-LEO footprint (equivalent area), R is the ERBE scene-dependent bidirectional model [Suttles *et al.*, 1988], and S is the spectral correction (equation (3)). Additional SZA dependence could not be explored since ScaRaB observed the area with only high solar elevations ($\text{SZA} < 45^\circ$). Both R and S depend on the scene (ERBE cloud category retrieved from the Meteosat observation). Broadband and narrowband bidirectional reflectance models are only approximately equivalent. However, this assumption is partly justified by the results of Boer and Ramanathan [1997] using the Japanese geostationary satellite GMS-4. They found a good agreement between their computed GEO-NB model and the ERBE model. Linear regressions are derived separately for each geotype (desert, land, ocean). All the near-coincident data ($\pm 6 \text{ mn}$) were used, but highly sampled (one column each 20 with a random start each line). The results are shown in Table 6. The flux RMS differences are large ($35\text{--}45 \text{ Wm}^{-2}$) compared to the VIS/SW ScaRaB comparisons (15 Wm^{-2}), no doubt due to the coregistration errors (space and time) inherent in using two instruments on different platforms.

[18] The same Meteosat-5 flux conversion method has then been applied to CERES/TRMM and CERES/Terra; the conclusions are presented in Table 7. Because the impact of mismatch errors is so high for the 10-km resolution of TRMM (see Table 2), homogeneity constraints have been applied. The first lines show, for ScaRaB data, the difference with or without such constraints: the RMS differences from the flux retrieval decrease from around 43 Wm^{-2} to 30 Wm^{-2} , but the mean bias also changes by 3 Wm^{-2} . With other tests on the sampling conditions for the same data set, we have observed that the variability of the bias was about 4 Wm^{-2} , which fixes at 2% the limit of accuracy of such intercomparisons by regression analysis. For comparison, the last columns show the results of a simple regression (neither angular nor NB-BB corrections). In all the cases,

Table 5. Correlation Between the Estimated Fluxes From the SW and Visible Channels of ScaRaB With or Without Spectral and Angular Correction^a

SW Flux Retrieval From	Spectral Correction	Angular Correction	r	RMS Differences, Wm^{-2}
SW radiance		no	0.992	19.47
Visible radiance	no	no		26.08
Visible radiance	no	yes	0.991	20.99
Visible radiance	yes	no	0.990	22.03
Visible radiance	yes	yes	0.995	14.98

^aFor March 1999, $N = 681\ 853$; mean flux = 229 Wm^{-2} .

Table 6. Linear Fit (Equation (3)) Between the SW ScaRaB Fluxes and the Meteosat-5 Visible Channel Numerical Count for March 19991

	Mean, $\text{Wm}^{-2}\text{sr}^{-1}$	<i>A</i>	<i>B</i>	<i>r</i>	RMS, $\text{Wm}^{-2}\text{sr}^{-1}$
Desert	285.6	1.472	-0.73	0.926	36.48
Land	239.6	1.411	14.98	0.946	35.55
Ocean	170.7	1.393	15.76	0.946	44.97

the corrections improve the correlation, but the differences are subtle: from 44.01 to 43.17 (ScaRaB case without homogeneity constraint). They are masked by the large background noise which results from the mismatch errors ($14\text{--}40 \text{ Wm}^{-2}$, Table 2) and residual NB-BB errors (15 Wm^{-2} , Table 5). Again, the SZA dependence could not be tested with observations at large solar zenith angles, except for CERES/TRMM in 2000. In that case, separated regressions for 3 SZA cases ($<45^\circ$, 45° to 60° , $>60^\circ$) useful for the monthly means computations were carried out but did not provide significant error reductions. Overall, the biases of the intercomparisons between five different SW instruments are very consistent (Table 7, column 4). Given the same homogeneity constraints, the mean bias compared to the case without homogeneity constant is -6.8 Wm^{-2} and the largest difference around this bias is 4.7 Wm^{-2} (2.4%). The three CERES instruments operating in March 2000 give notably close results, although the viewing geometry was different (large variety of solar zenith angles for PFM/TRMM, large variety of solar azimuth angles for FM1/Terra in rotating azimuth mode). Although at the limit of accuracy discussed above (2%), the +1.3% difference between ScaRaB and CERES is consistent with the results of *Haeffelin et al.* [2001]. The -2% difference between CERES 1999 and 2000 may be linked to the degradation of the Meteosat sensor in the course of one year (-1.4% per year according to the trend of the vicarious calibration coefficient documented at www.eumetsat.de).

5. Combined CERES-Meteosat-5 Monthly Means

5.1. The LW Domain

[19] Except at high latitude, a satellite in a near polar orbit observes a particular region only twice in 24 hours. In the ERBE-type processing, the instantaneous regional means are interpolated or extrapolated throughout the day to all local times (values at the local half-hour, e.g., 0030, 0130,

etc.), using the algorithms described by *Brooks et al.* [1986]. The radiant flux interpolation is linear over ocean and snow-ice, but uses a daytime half-sine fit over land/desert and coastal scenes. Region by region, the estimated local hourly radiant fluxes are then averaged to compute the daily means, the monthly mean diurnal variation, and the overall monthly means. With Meteosat-5, observations are available at each half-hour, and we have shown that the LW fluxes can be estimated with high accuracy thanks to equation (1). Consequently, we have used all the half-hour observations (IR and WV radiances) of the month, converted them to fluxes using equation (1), and computed the arithmetic average. Special care has to be devoted to missing or spurious slots (eliminated with the bad-line flag). In summary, although the CERES data are not directly used, they have served to check the flux conversion equation. Therefore the monthly means computations depend first on the CERES radiometric calibration and second on Meteosat-5 for the diurnal corrections.

[20] The differences between the Meteosat and the ERBE-type CERES monthly means (ES4, Ed.1) are shown on Figure 3. The regional differences spread over a surprisingly small range ($\pm 10 \text{ Wm}^{-2}$), even though the monthly mean diurnal cycle has amplitudes greater than 40 Wm^{-2} over certain areas. The average of day and night CERES observations is then a good representation of the full 24-hour cycle. The spatial patterns of the differences are not random, but the observed structures cannot be easily linked to VZA, nor can they be easily linked either to cloud or to water vapor variations. The tropical mean difference over the considered longitudes is close to zero (-2 Wm^{-2}).

5.2. The SW Domain

[21] In the SW domain, only one daytime observation is generally available per 24-hour period. In the ERBE-type processing, each instantaneous regional average is adjusted to the local half-hours, taking into account modeled directional albedo [*Suttles et al.*, 1988] for each scene type and differences of Sun elevation [*Brooks et al.*, 1986]. If at least two SW observations are available, two series of extrapolated fluxes are computed, and the flux is linearly interpolated between the two observation hours. Except when several observations are available in the day, the ERBE-type method is thus based on the assumption of diurnally constant cloud conditions. *Standfuss et al.* [2001] have used this approach and have introduced adjustments based on a

Table 7. Regression Results Between the ScaRaB or CERES and the Meteosat-5 SW Flux Estimates

Instrument	Population Size	Flux Mean, Wm^{-2}	Differences: ScaRaB or CERES Minus Meteosat Flux Estimates					
			Regression With Spectral and Angular Correction ^a			Simple Regression ^b		
			Mean	<i>r</i>	RMS	<i>r</i>	RMS	
ScaRaB 1999 03	7909	207.1	0.819	0.947	43.18	0.945	44.01	
Same but with homogeneity constraints	3480	211.28	-1.99	0.987	22.69	0.982	26.63	
TRMM 1999 03	15456	191.99	-5.5	0.966	45.62	0.956	52.14	
TRMM 2000 03-4 days	9334	217.78	-7.84	0.976	41.69	0.969	48.03	
TERRA FM1 2000 03 11 days	13962	218.9	-9.4	0.975	38.39	0.955	51.17	
TERRA FM2 2000 03 12 days	14795	232.9	-9.35	0.981	35.67	0.971	43.37	

^aFrom equation (3).

^bNo spectral, no angular correction.

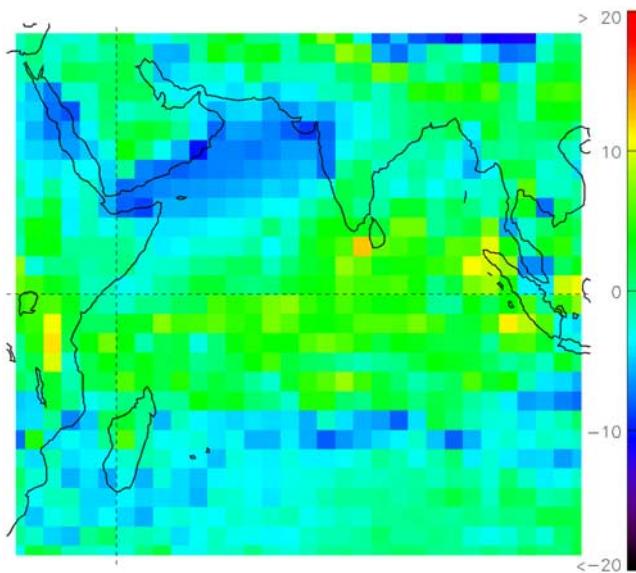


Figure 3. Difference between the CERES-Meteosat combination and the ERBE-type LW CERES monthly means for March 2000 (Wm^{-2}).

regional diurnal albedo climatology computed from five years of ERBS scanner data (November 1985 to February 1990). However, it is expected that better correction will be obtained with the planned filling of temporal gaps using direct contemporary observations. As an example *Haefelin et al.* [1999] used the contemporary cloud reflectances found in the ISCCP C1 (former version of D1) cloud radiances to improve the accuracy of ERBE monthly means. And, based on methods described by *Young et al.* [1998], the advanced CERES processing, now in validation phase, uses 3-hourly radiance and cloud property data from geostationary imagers. The narrowband-broadband relationship is based on comparisons between CERES and the imager on the same platform [*Minnis et al.*, 2002a]. Fluxes are computed using the CERES ADM [*Loeb et al.*, 2003] and normalized to the CERES observations. In the present work with basically the same approach, we estimate SW fluxes at each half-hour from the Meteosat-5 narrow-band data using equation (4) and the appropriate regression coefficients. To determine the Meteosat-based monthly means, we did not directly compute the arithmetic average of all the flux estimates as in the LW domain, for two reasons. First, the uncertainties of the instantaneous fluxes are larger in the SW than in the LW domain. Second, for a given time slot, local solar time varies continuously over the Meteosat image; as a result, direct averaging would combine imperfectly defined local half-hours, significantly affected by the strong SZA dependence of the albedo. A rough image averaging may also contain spurious data during twilight and nighttime. Instead, we use the Meteosat data to fill in the 31×24 day-hour matrix of albedo for the ERBE 2.5° region. Depending on the local time of observation, all the Meteosat albedo estimates are adjusted to the local half-hours taking into account the difference of solar zenith angle. Thus we use the ERBE-like data processing, but substituting the Meteosat-derived albedo (except in the case of absent or spurious data) for the time-interpolated albedo. In other words, the daily means are computed with the

original CERES instantaneous flux estimates and the shape of the albedo diurnal variation observed by Meteosat. In this way, residual NB-BB and angular conversion errors are minimized, while the actual diurnal variations of cloudiness on the day of observation are effectively taken into account. The differences between the Meteosat-based and CERES monthly means are shown on Figure 4, and examples of monthly mean diurnal cycles are given in Figures 5 and 6. Figure 4 shows that the regional corrections range from about -20 to $+20 \text{ Wm}^{-2}$. Negative corrections are observed in the southern part of Africa, in the southeast of the Indian Ocean, and over China. They are typical for predominant morning cloudiness, with albedo greater in the morning than in the afternoon (Figure 5). Positive corrections (in red) are observed in the area of the African great lakes, over Indonesia, and over ocean northwest of Madagascar (near the Seychelles islands, at the northern edge of the ITCZ). When averaging over the 20°S – 20°N zone, negative and positive corrections are largely balanced. However, the mean difference is significantly different from zero, around $+4 \text{ Wm}^{-2}$.

6. Conclusions

[22] In this study, we have evaluated the accuracy improvement obtained in determinations of daily variations and monthly means of the broadband TOA ERB components, using geostationary narrow-band data to complete the imperfect time sampling corresponding to a BBSR operating on only one or two satellites in low Earth orbit. This was the case during most of the Nimbus, ERBE, ScaRaB, and CERES missions. Note that broadband radiance data can be obtained from geostationary satellites, but only one such instrument (GERB on MSG-1 [*Harries and Crommelynck*, 1999]), observing only part of the globe with fixed viewing geometry, is currently in operation. Our results are summarized as follows.

[23] 1. Intercomparison with simultaneous collocated ScaRaB-2 data has made it possible to compute broadband flux estimates from the Meteosat-5 narrow-band radiances.

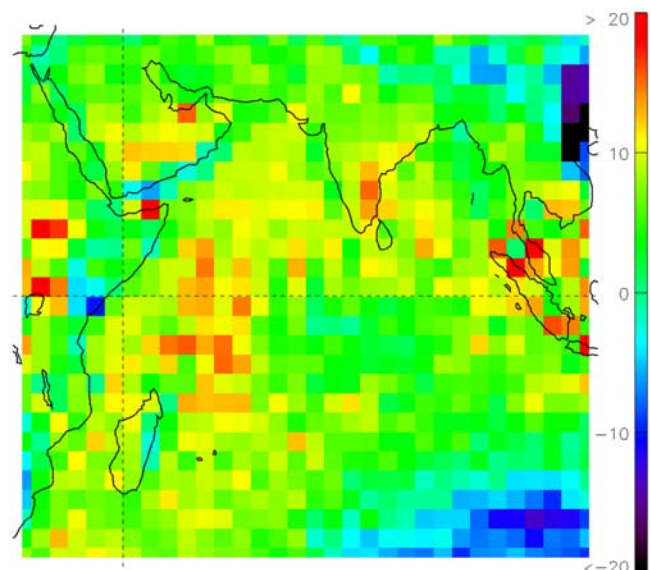


Figure 4. Same as Figure 3, but for the SW domain.

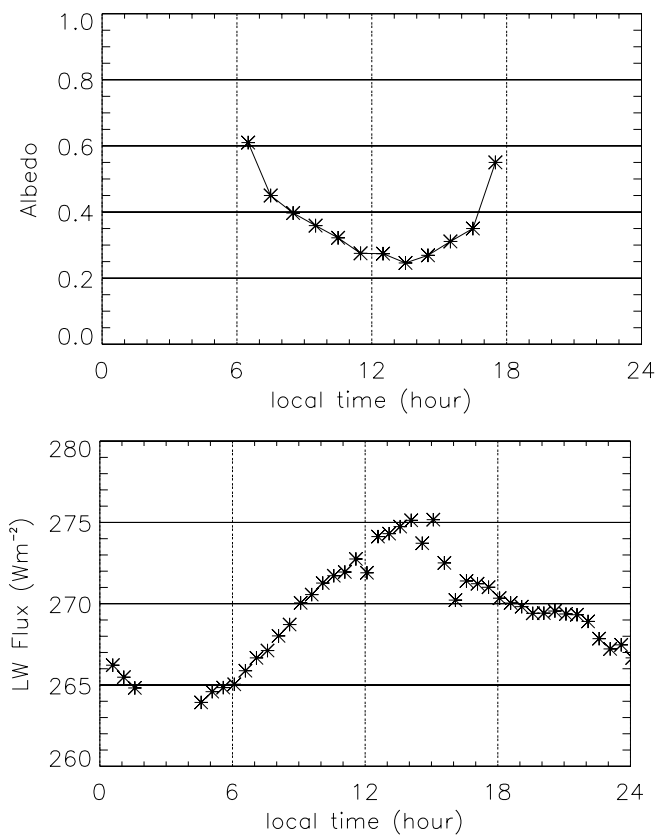


Figure 5. Area of predominant morning cloudiness: monthly means of the diurnal cycle for albedo (top) and LW flux (bottom), over ocean west of Australia (longitude = 104°E , latitude = 29°S).

The same formula with identical coefficients has been used to compare the Meteosat-5 fluxes to CERES-PFM results for March 1999 and 2000, and to CERES FM1 and FM2 results for March 2000. The observed differences correspond to biases less than 1% and 4% respectively in the LW and SW. Such small biases are remarkable and demonstrate the excellent radiometric stability of the five instruments (the Meteosat-5 scanner, ScaRaB, and CERES PFM, FM1, and FM2 scanners).

[24] 2. The corresponding RMS differences between the BBSR-LEO and NBI-GEO instantaneous flux estimates remain very large, especially in the SW (40 Wm^{-2} , or 10%), and the improvement due to angular and NB-BB conversions exists but is very subtle. In fact, the initial noise due to mismatch errors (which we estimate at 20 Wm^{-2}) makes it very hard to interpret the relationship between BBSR-LEO and NBI-GEO radiances and fluxes. The combined localization errors of the two data sets are about 15 km and probably cannot be reduced further on an operational basis. As a result, improvement of BBSR-LEO instantaneous flux estimates by combination with NBI-GEO data is highly unlikely.

[25] 3. The main interest of the BBSR-LEO/NBI-GEO combination then remains in the improvement of temporal means. The Meteosat-5 fluxes have been used to fill the gaps between the 10:30 CERES/Terra observations and to take into account the real diurnal variation of cloudiness and other atmospheric parameters. The differences introduced

by these new calculations are small in the LW domain: the “average” of the day and night CERES/Terra LW observations yields an approximately correct monthly mean, despite the strong diurnal cycle, specifically over areas of deep convection. However, in the SW domain, the differences are more significant (regional mean differences $\sim 20\text{ Wm}^{-2}$, tropical mean differences $\sim 4\text{ Wm}^{-2}$), although the 10:30 observation time, not far from noon, was favorable for daily averaging. Note that, compared to the ERBE record, there was a decrease of about -3% in the 1994–1997 tropical mean reflected SW found in the ERBS nonscanner records, continuing after 1997 according to the CERES/TRMM data [Wielicki *et al.*, 2002, Figures 2 and 3]. After 2000, with the CERES/Terra ES4 data, the difference reaches -5 to -6% . Neither TRMM nor ERBS data should be subject to the strong time-sampling bias of the Sun-synchronous satellites. However, although limited to longitudes 30 to 110° West, our results suggest that diurnal cycle bias for CERES/Terra may be as strong as -3% . Applying such a correction, and leaving aside the strong post-Pinatubo (1991–92) and ENSO (1997–98) excursions, the CERES/Terra SW tropical mean reflected SW flux may exhibit rough constancy since 1994 of the negative anomaly (-3% compared to ERBE prior to 1991), determined from ERBE/ERBS, ScaRaB-1 and -2, and CERES/TRMM data. The analysis of the broadband radiances of GERB on MSG-1 [Harries and Crommelynck, 1999], and the accurate GEO interpolation of CERES [Young *et al.*, 1998] should definitively

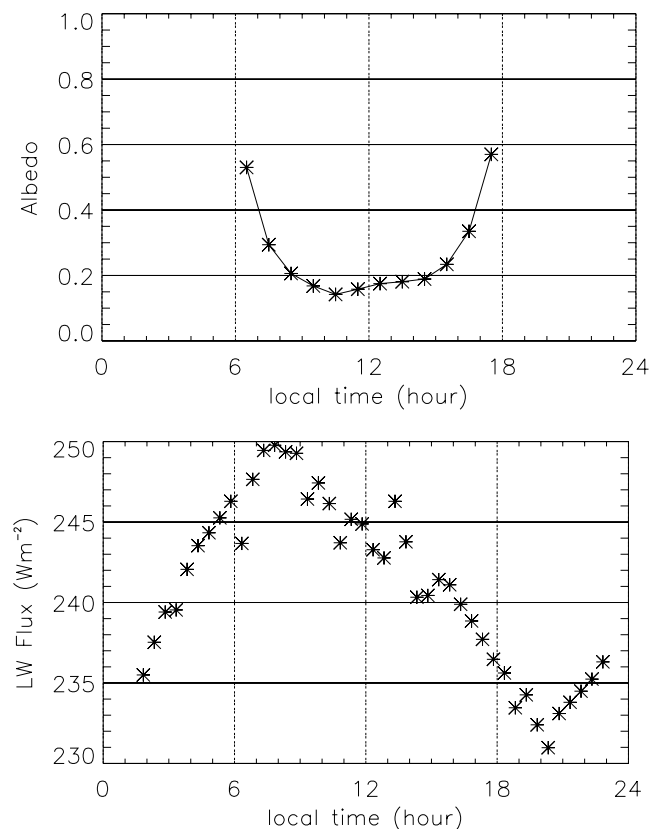


Figure 6. Same but for region of predominant afternoon cloudiness, over ocean northwest of Madagascar (longitude = 56°E , latitude = 6°S).

settle this important issue of the Earth Radiation Budget observations.

[26] **Acknowledgments.** The CERES data were obtained from the NASA Langley Research Center Atmospheric Sciences Data Center. The Meteosat-5 data were supplied by Eumetsat, and the storage and processing facilities were provided by the Climserv database (Jean Louis Monge at LMD, <http://climserv.lmd.polytechnique.fr>).

References

- Barkstrom, B. R., E. F. Harrison, G. L. Smith, R. Green, J. Kibler, R. Cess, and ERBE Science Team (1989), Earth Radiation Budget Experiment (ERBE) archival and April 1985 results, *Bull. Am. Meteorol. Soc.*, *70*, 1254–1262.
- Boer, E. R., and V. Ramanathan (1997), Lagrangian approach for deriving cloud characteristics from satellite observations and its implications to cloud parameterization, *J. Geophys. Res.*, *102*, 21,383–21,399.
- Brest, C. L., W. B. Rossow, and M. D. Roiter (1997), Update of radiance calibrations for ISCCP, *J. Atmos. Oceanic Technol.*, *14*, 1091–1109.
- Brooks, D. R., E. H. Harrison, P. Minnis, J. T. Suttles, and R. Kandel (1986), Development of Algorithms for understanding the temporal and spatial variability of Earth's radiation balance, *Rev. Geophys.*, *24*, 422–438.
- Buriez, J. C., C. Vanbauce, F. Parol, P. Gouloub, M. Herman, B. Bonnel, Y. Fouquart, P. Couvert, and G. Sèze (1997), Cloud detection and derivation of cloud properties from POLDER, *Int. J. Remote Sens.*, *18*, 2785–2813.
- Cheruy, F., R. S. Kandel, and J. P. Duvel (1991a), Outgoing longwave radiation and its diurnal variation from combined ERBE and Meteosat observations: 1. Estimating OLR from Meteosat data, *J. Geophys. Res.*, *96*, 2611–2622.
- Cheruy, F., R. S. Kandel, and J. P. Duvel (1991b), Outgoing longwave radiation and its diurnal variation from combined ERBE and Meteosat observations: 2. Using Meteosat data to determine the LW diurnal cycle, *J. Geophys. Res.*, *96*, 2623–2630.
- Desormeaux, Y., W. B. Rossow, C. L. Brest, and G. G. Campbell (1993), Normalization and calibration of Geostationary Radiances for the International Satellite Cloud Climatology Project, *J. Atmos. Oceanic Technol.*, *10*, 304–325.
- Dewitte, S. (1997), Local instantaneous radiation budget, measured from geostationary and polar satellites, Ph.D. dissertation, Vrije Univ. eit Brussel, Brussels.
- Dewitte, S., P. Boekaerts, and F. Sirou (1999), Determination of the ScaRaB FM1 broadband channel point spread functions, *IEEE Trans. Geosci. Remote Sens.*, *37*(4), 2004–2010.
- Diekmann, F. J., and G. L. Smith (1989), Investigation of scene identification algorithms for radiation budget measurements, *J. Geophys. Res.*, *94*, 3395–3412.
- Diner, D. J., G. P. Asner, R. Davies, Y. Knyazikhin, J. P. Muller, A. W. Nolin, B. Pinty, C. B. Schaaf, and J. Stroeve (1999), New directions in Earth observing: Scientific applications of multiangle remote sensing, *Bull. Am. Meteorol. Soc.*, *80*, 2209–2228.
- Dlhopsky, R., A. Macke, and R. Stuhlmann (1994), A study of improved angular dependence models for radiation field measurements aboard future satellites, *Final Rep. ESA, contract AO/1-2562/91/NL/SF*, Eur. Space Ag., Paris.
- Duvel, J. P., and P. Raberanto (2000), A geophysical cross-calibration approach for broadband channels: Application to the ScaRaB experiment, *J. Atmos. Oceanic Technol.*, *17*, 1609–1717.
- Duvel, J. P., S. Bouffies-Cloch e, and M. Viollier (2000), Determination of shortwave Earth reflectances from visible radiance measurements: Error estimate using ScaRaB data, *J. Appl. Meteorol.*, *39*, 957–970.
- Duvel, J. P., M. Viollier, P. Raberanto, R. Kandel, M. Haeffelin, L. A. Pakhomov, V. A. Golovko, J. Mueller, R. Stuhlmann, and the International ScaRaB Scientific Working Group (ISSWG) (2001), The ScaRaB-Resurs Earth radiation budget dataset and first results, *Bull. Am. Meteorol. Soc.*, *82*, 1397–1408.
- Haeffelin, M., R. Kandel, and C. Stubenrauch (1999), Improved diurnal interpolation of reflected broad-band shortwave observations using ISCCP data, *J. Atmos. Oceanic Technol.*, *16*, 38–54.
- Haeffelin, M., B. A. Wielicki, J. P. Duvel, K. Priestley, and M. Viollier (2001), Intercalibration of CERES and ScaRaB Earth radiation budget datasets using temporally and spatially collocated radiance measurements, *Geophys. Res. Lett.*, *28*(1), 167–170.
- Harries, J. E., and D. Crommelynck (1999), The geostationary Earth radiation budget experiment on MSG-1 and its potential applications, *Adv. Space Res.*, *24*(7), 915–919.
- House, F. B., A. Gruber, G. E. Hunt, and A. T. Mecherikunnel (1986), History of satellite missions and measurements of the Earth radiation budget, *Rev. Geophys.*, *24*, 357–377.
- Kandel, R., et al. (1998), The ScaRaB Earth radiation budget dataset, *Bull. Am. Meteorol. Soc.*, *79*, 765–783.
- Li, Z., and H. G. Leighton (1992), Narrowband to broadband conversion with spatially autocorrelated reflectance measurements, *J. Appl. Meteorol.*, *31*, 653–670.
- Li, Z., and A. Trishchenko (1999), A study towards an improved understanding of the relation between visible and SW albedo measurements, *J. Atmos. Oceanic Technol.*, *17*, 347–360.
- Loeb, N. G., F. Parol, J. C. Buriez, and C. Vanbauce (2000), Top of the atmosphere albedo estimation from angular distribution models using scene identification from satellite cloud property retrievals, *J. Clim.*, *13*, 1269–1284.
- Loeb, N. G., N. M. Smith, S. Kato, W. F. Miller, S. K. Gupta, P. Minnis, and B. A. Wielicki (2003), Angular distribution models for top-of-atmosphere radiative flux estimation for the clouds and the Earth's radiant energy system instrument on the Tropical Rainfall Measuring Mission Satellite, part 1: Methodology, *J. Appl. Meteorol.*, *42*, 240–265.
- Minnis, P., D. F. Young, and E. F. Harrison (1991), Examination of the relationship between outgoing infrared window and total longwave fluxes using satellite data, *J. Clim.*, *4*, 1114–1133.
- Minnis, P., L. Nguyen, D. R. Doelling, D. F. Young, W. F. Miller, and D. P. Kratz (2002a), Rapid calibration of operational and research meteorological satellite imagers. Part I: Evaluation of research satellite visible channels as references, *J. Atmos. Oceanic Technol.*, *19*, 1233–1249.
- Minnis, P., L. Nguyen, D. R. Doelling, D. F. Young, W. F. Miller, and D. P. Kratz (2002b), Rapid calibration of operational and research meteorological satellite imagers. Part II: Comparison of infrared channels, *J. Atmos. Oceanic Technol.*, *19*, 1250–1266.
- Roca, R., M. Viollier, L. Picon, and M. Desbois (2002), A multisatellite analysis of deep convection and its moist environment over the Indian Ocean during the winter monsoon, *J. Geophys. Res.*, *107*(D19), 8012, doi:10.1029/2000JD000040.
- Standfuss, C., M. Viollier, R. S. Kandel, and J. P. Duvel (2001), Regional diurnal albedo climatology and diurnal time extrapolation of reflected solar flux observations, application to the ScaRaB record, *J. Clim.*, *14*, 1129–1146.
- Stubenrauch, C., J. P. Duvel, and R. S. Kandel (1993), Determination of longwave anisotropic emission factors from combined broad- and narrow-band radiance measurements, *J. Appl. Meteorol.*, *32*, 848–856.
- Stubenrauch, C. J., V. Briand, and W. B. Rossow (2002), The role of clear sky identification in the study of cloud radiative effects: Combined analysis from ISCCP and the Scanner of Radiation Budget (ScaRaB), *J. Appl. Meteorol.*, *41*, 396–412.
- Suttles, J. T., R. N. Green, P. Minnis, G. L. Smith, W. F. Staylor, B. A. Wielicki, I. J. Walker, D. F. Young, V. R. Taylor, and L. L. Stowe (1988), Angular radiation models for Earth-atmosphere system, vol. 1, Shortwave radiation, *NASA Ref. Publ. 1184*, Greenbelt, Md.
- Thomas, D., J.-P. Duvel, and R. Kandel (1995), Diurnal bias in calibration of broad-band radiance measurements from space, *IEEE Trans. Geosci. Remote Sens.*, *33*, 670–683.
- Trishchenko, A., and Z. Li (1998), Use of ScaRaB measurements for validating a GOES-based TOA radiation product, *J. Appl. Meteorol.*, *37*, 591–605.
- Vesperini, M., and Y. Fouquart (1994), Determination of broadband shortwave fluxes from the Meteosat visible channel by comparison to ERBE, *Beitr. Phys. Atmos.*, *67*(2), 121–132.
- Viollier, M., R. Kandel, and P. Raberanto (1995), Inversion and space-time averaging algorithms for ScaRaB (Scanner for Earth Radiation Budget)—Comparison with ERBE, *Ann. Geophys.*, *13*, 959–968.
- Wielicki, B. A., and R. N. Green (1989), Cloud identification for ERBE radiative flux retrieval, *J. Appl. Meteorol.*, *28*, 1133–1146.
- Wielicki, B. A., B. R. Barkstrom, E. F. Harrison, R. B. Lee III, G. L. Smith, and J. E. Cooper (1996), Clouds and the Earth's radiant energy system (CERES): An Earth Observing System experiment, *Bull. Am. Meteorol. Soc.*, *77*, 853–868.
- Wielicki, B. A., et al. (2002), Evidence for large decadal variability in the tropical mean radiative energy budget, *Science*, *295*, 841–844.
- Ye, Q., and J. A. Coakley Jr. (1996), Biases in Earth radiation budget observations: 2. Consistent scene identification and anisotropic factors, *J. Geophys. Res.*, *101*, 21,253–21,263.
- Young, D. F., P. Minnis, D. R. Doelling, G. G. Gibson, and T. Wong (1998), Temporal interpolation methods for the Clouds and the Earth's Radiant Energy System (CERES) experiment, *J. Clim. Appl. Meteorol.*, *37*, 572–590.

R. Kandel, P. Raberanto, and M. Viollier, Laboratoire de M eteorologie Dynamique, IPSL, CNRS, Ecole Polytechnique, F-91128 Palaiseau Cedex, France. (viollier@lmd.polytechnique.fr)